

Effect of the relative phase between pre-existing 2/1 and 3/1 magnetic islands on the suppression of runaway electrons on J-TEXT

Jin-Yu Xiong(熊金玉), Zhong-He Jiang(江中和), Zi-Xiao Jiao(焦子啸), Zhen Li(李振),Yun-Feng Liang(梁云峰), Zhong-Yong Chen(陈忠勇), Yong-Hua Ding(丁永华), and J-TEXT Team

Citation: Chin. Phys. B, 2023, 32 (**7**): 075210. DOI: 10.1088/1674-1056/acc3f9
Journal homepage: http://cpb.iphy.ac.cn; http://iopscience.iop.org/cpb

What follows is a list of articles you may be interested in

Drift surface solver for runaway electron current dominant equilibria during the current quench

Lu Yuan(袁露) and Di Hu(胡地)
Chin. Phys. B, 2023, 32 (**7**): 075208. DOI: 10.1088/1674-1056/acc1d7

Effect of tearing modes on the confinement of runaway electrons in Experimental Advanced Superconducting Tokamak

Rui-Jie Zhou(周瑞杰)
Chin. Phys. B, 2023, 32 (**7**): 075204. DOI: 10.1088/1674-1056/acc3f8

Observation of trapped and passing runaway electrons by infrared camera in the EAST tokamak

Yong-Kuan Zhang(张永宽), Rui-Jie Zhou(周瑞杰), Li-Qun Hu(胡立群), Mei-Wen Chen(陈美文), Yan Chao(晁燕), Jia-Yuan Zhang(张家源), and Pan Li(李磐)
Chin. Phys. B, 2021, 30 (**5**): 055206. DOI: 10.1088/1674-1056/abd758

Effects of resonant magnetic perturbation on the instability of single tearing mode with non-shear flow

Le Wang(王乐), Ming Yang(阳明), Wen-Bin Lin(林文斌)
Chin. Phys. B, 2019, 28 (**1**): 015203. DOI: 10.1088/1674-1056/28/1/015203

Synchrotron radiation intensity and energy of runaway electrons in EAST tokamak

Y K Zhang(张永宽), R J Zhou(周瑞杰), L Q Hu(胡立群), M W Chen(陈美文), Y Chao(晁燕), EAST team
Chin. Phys. B, 2018, 27 (**5**): 055206. DOI: 10.1088/1674-1056/27/5/055206

SPECIAL TOPIC — Plasma disruption

Effect of the relative phase between pre-existing 2/1 and 3/1 magnetic islands on the suppression of runaway electrons on J-TEXT

Jin-Yu Xiong(熊金玉)[1,2], Zhong-He Jiang(江中和)[1,†], Zi-Xiao Jiao(焦子啸)[1], Zhen Li(李振)[1], Yun-Feng Liang(梁云峰)[1,3,4], Zhong-Yong Chen(陈忠勇)[1], Yong-Hua Ding(丁永华)[1], and J-TEXT Team[1]

[1] *International Joint Research Laboratory of Magnetic Confinement Fusion and Plasma Physics, State Key Laboratory of Advanced Electromagnetic Engineering and Technology, School of Electrical and Electronic Engineering, Huazhong University of Science and Technology, Wuhan* 430074, China

[2] *Yangtze Memory Technologies Co., Ltd., Wuhan* 430074, China

[3] *Institute of Plasma Physics, Chinese Academy of Sciences, Hefei* 230031,China

[4] *Forschungszentrum Jülich GmbH, Institut für Energie-und Klimaforschung-Plasmaphysik, Jülich* 52425, Germany

(Received 29 December 2022; revised manuscript received 27 February 2023; accepted manuscript online 14 March 2023)

In the experiments of actively triggering plasma disruption by massive gas injection, the externally applied resonant magnetic perturbation has been used to mitigate the hazard of runaway electron (RE). Motivated by the experiment of multimode coupling to suppress REs on J-TEXT, some typical simulation cases with non-ideal MHD with rotation-open discussion (NIMROD) code are carried out to explore the influential mechanism of different relative phases between $m/n = 2/1$ and $m/n = 3/1$ magnetic islands on the confinement of REs. Results show that the RE confinement is drastically affected by the relative phase between $2/1$ and $3/1$ magnetic islands. When the O point phase of $2/1$ and $3/1$ magnetic islands is toroidal 330°, REs can be effectively lost. The fitting curve of the remaining ratio of REs vs. the relative toroidal phase is predicted to approximate a sine-like function dependence. Further studies indicate that the phase difference between coexisting $2/1$ and $3/1$ islands can affect the radial transport of impurities. The loss of runaway electrons is closely related to the deposition effect of impurity. The impurity is easier to spread into the core region with smaller poloidal phase difference between the radial velocity of impurity and the impurity quantity of Ar.

Keywords: major disruption, runaway electron, massive gas injection (MGI), resonant magnetic perturbation (RMP)

PACS: 52.65.Kj, 52.25.Fi, 52.25.Vy, 47.65.–d **DOI:** 10.1088/1674-1056/acc3f9

1. Introduction

In the process of tokamak discharge, a variety of magnetohydrodynamic (MHD) instabilities may cause disruption, which terminates the plasma discharge suddenly.[1,2] Once the plasma disruption of tokamaks takes place, a lot of heat and magnetic energy are rapidly lost in milliseconds, causing serious damage to the device that includes three aspects: heat loads of vacuum vessel wall and divertor target plates, electromagnetic force of vacuum vessel wall, and generation of runaway current.[3–5] Among these damages, the high-flux and high-energy runaway electrons (REs) produced in the process of plasma disruption cause fateful hazards on the device wall.[5] Therefore, the International Thermonuclear Experimental Reactor (ITER) and future fusion reactors need reliable mitigation methods to suppress or dissipate runaway current during the plasma disruption.[6,7]

The high toroidal electric field produced during the plasma disruption contributes to RE generation, and results indicate that the generation of REs can be suppressed by increasing the plasma density and the collision frequency between high-energy electrons and bulk plasma to decrease the growth rate of electron energy.[8] Based on the above mentioned principles, the massive gas injection (MGI) or shattered pellet injection (SPI) is used to increase the plasma density.[9–12] At the same time, the cooling effect of high Z impurity can trigger the MHD instability and enhance the magnetic perturbation amplitude of plasma. Thus, most of time, the generation of REs can be efficiently suppressed. Related experiments with noble gas MGI have been conducted on several devices, such as Tore Supra,[13] ASDEX Upgrade,[14] TEXTOR,[15] DIII-D,[16] and J-TEXT.[17] Results demonstrate that the enhancement of electron density can increase the critical electric field and effectively prevent the generation of REs. However, in theory, the complete suppression of REs should require the plasma density to reach the Rosenbluth density.[18] However, the increased density by MGI and SPI is still far from the density threshold. To date, the complete suppression of REs by the mass impurity injection is still open.

Another alternative scheme of RE mitigation is the enhancement of magnetic perturbations of plasma with the externally applied resonant magnetic perturbation (RMP).[19,20] The large magnetic perturbation amplitude of plasma can lead to remarkable magnetic surface stochasticity and result in an

[†]Corresponding author. E-mail: zhhjiang@hust.edu.cn

© 2023 Chinese Physical Society and IOP Publishing Ltd

enhanced orbit loss of REs before the avalanche process can amplify the RE seeds during the current quench (CQ) stage of disruption. At present, experiments on the application of RMP for runaway current mitigation have been carried out on many devices, such as DIII-D,[21] TEXTOR,[22] JT-60U,[23] ASDEX Upgrade,[24] and J-TEXT.[25] The application of $n = 3$ RMP fields prior to the onset of thermal quench (TQ) may suppress the runaway current on DIII-D with apparently high effectiveness in diverted plasmas. The generation of REs is suppressed in TEXTOR disruptions by applying perturbation fields with $n = 1$ and $n = 2$ RMP fields. The experimental results on ASDEX upgrade show that the runaway current is remarkably reduced with dominant toroidal mode number $n = 1$ RMP fields applied by B-coils. The use of RMP to suppress REs has also been studied on the J-TEXT tokamak. The runaway current can be suppressed with mode locking by the application of $m/n = 2/1$ RMP fields before the TQ.[26] In the meantime, dominant multi-modes (such as $3/1$ and $2/1$ modes) of RMP are applied to suppress REs on J-TEXT.[27] Partial experiment results show that the phase and amplitude of the two modes have important influences on RE suppression, but unfortunately, the phase adjustment range of the J-TEXT between the two modes on RMP files is limited. Experimental results motivate us to study the RE suppression of double dominant modes of RMP with the numerical simulation. In contrast to our previous work,[28] this work focuses on the effects of RMP-induced multimode coupling on RE suppression.

In the rest of this paper, the results of simulation have been presented, which is Ar MGI for target plasmas in the presence of pre-existing $2/1$ and $3/1$ magnetic islands performed with the NIMROD code on J-TEXT. Section 2 describes the applied computational model for the simulations. Section 3 presents the scanning results and relevant physical mechanism. Section 4 presents the concluding discussion and summary.

2. Computational model

The three-dimensional MHD code NIMROD is used to explore the transport of REs in this article.[29] For simulating the process of disruption triggered by MGI, the KPRAD module has been used in NIMROD, which calculates the process of ionization, recombination, and radiation for each impurity charge state.[30] The viscosity, μ, is 27 m^2/s, which is a bit larger for a typical J-TEXT plasma, but not affect the qualitative results. The perpendicular thermal diffusion in the simulation is defined by the initial values of χ of 0.1 m^2/s in the core and 1 m^2/s at the edge, and the parallel thermal diffusion is defined by the initial values of $\chi_\parallel$ of 1×10^8 m^2/s in the core and at the edge. The orbit model of test particles in KPRAD is used to track the trajectory of each RE and study the physical mechanism of MHD on the electron loss during disruption.[31] The equations of dynamic drift orbit and parallel velocity of RE are presented as follows:

$$\mathrm{d}R = \frac{v_\parallel B_R}{B}\mathrm{d}t + \frac{1}{B^2}[\boldsymbol{E}\times\boldsymbol{B}]_R\mathrm{d}t, \tag{1}$$

$$\mathrm{d}Z = \frac{v_\parallel B_Z}{B}\mathrm{d}t + \frac{1}{R}\frac{\gamma m_\mathrm{e} v_\perp^2}{2eB}\mathrm{d}t + \frac{1}{R}\frac{\gamma m_\mathrm{e} v_\parallel^2}{eB}\mathrm{d}t + \frac{1}{B^2}[\boldsymbol{E}\times\boldsymbol{B}]_Z\mathrm{d}t, \tag{2}$$

$$\mathrm{d}\varphi = \frac{v_\parallel B_\varphi}{RB}\mathrm{d}t + \frac{1}{RB^2}[\boldsymbol{E}\times\boldsymbol{B}]_\varphi\mathrm{d}t, \tag{3}$$

$$\begin{aligned}\mathrm{d}v_\parallel = &-\frac{eE_\parallel}{\gamma^3 m_\mathrm{e}}\mathrm{d}t + \frac{v_\perp^2 B_R}{2\gamma^2 BR}\mathrm{d}t \\ &-\frac{1}{\gamma^4}\frac{v_\parallel}{|v_\parallel|^3}\frac{e^4\ln\Lambda}{4\pi\varepsilon_0 m_\mathrm{e}^2}n_\mathrm{e}(Z_\mathrm{eff}+1+\gamma)\mathrm{d}t \\ &-\gamma v_\parallel^3\frac{e^2}{6\pi\varepsilon_0 m_\mathrm{e}c^3}\left(\frac{1}{R_0^2}+\frac{e^2B^2v_\perp^2}{\gamma^2 m_\mathrm{e}^2 v_\parallel^4}\right)\mathrm{d}t \\ &-\frac{1}{\gamma^2}\frac{e^4(Z_\mathrm{eff}+1)}{548\pi^2\varepsilon_0 m_\mathrm{e}^2c^2}n_\mathrm{e}\left(\ln(2\gamma)-\frac{1}{3}\right)\frac{v_\parallel}{|v_\parallel|}\mathrm{d}t.\end{aligned} \tag{4}$$

The drift orbit of REs includes the electric field, magnetic field gradient, and curvature drift terms. $v_\parallel$ and $v_\perp$ are the parallel and perpendicular velocities, respectively, along the magnetic field line; γ is a relativistic factor, $\ln\Lambda$ is the Coulomb logarithm, and the local effective charge number $Z_\mathrm{eff} = \sum n_i Z_i^2/n_\mathrm{e}$. B is the total magnetic field, it includes both of the toroidal and poloidal fields in NIMROD. The simulation results are in good agreement with the experimental results on DIII-D and J-TEXT.[28,31,32] This model can make us easily predict the confinement time, hit position, and transport process of RE.

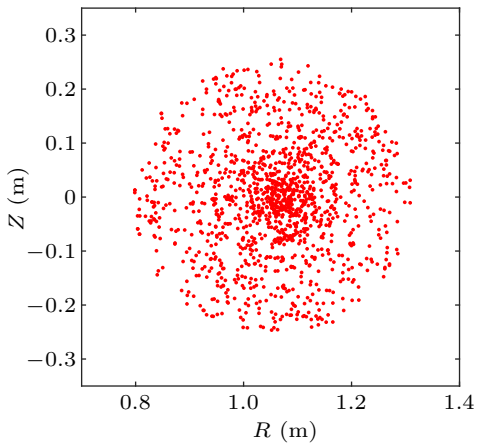


Fig. 1. Initial position distribution of REs in a plasma poloidal surface.

The input physical parameters in this paper are given by the equilibrium file, which is based on experimental data of J-TEXT. The two-dimensional equilibrium of plasma is given by the EFIT equilibrium reconstruction code. The equilibrium file contains plasma current ($I_\mathrm{p} = 150$ kA), toroidal field

($B_t = 1.75$ T), pressure profile, safety factor profile, magnetic flux, limiter information, and grid position information. The rest of the information needs to be given in the input parameter file of NIMROD. Given that the mechanism of generation of REs is not involved in NIMROD, 920 test REs with a certain initial velocity (150 keV) are randomly distributed in the plasma region in the initial stage of impurity gas injection (Fig. 1), and the pitch angle of electrons is fixed at 10°.

3. Computational results

3.1. Effect of the relative phase between pre-existing 2/1 and 3/1 magnetic islands on the suppression of REs

The $2/1$ and $3/1$ magnetic islands in all calculating cases are pre-existing, and their corresponding amplitudes are 30 Gs and 10 Gs, respectively, to ensure that the simulation conditions are similar to the experimental conditions. The impurity gas of Ar is injected continuously for 0.1 ms from the initial time at a constant gas injection rate. In NIMROD, the MGI source is simply set with the following formula:

$$n_{\rm imp} = n_{\rm max}\exp(-(\theta/15)^2)\exp(-(\varphi/60)^2), \tag{5}$$

where θ and φ are the poloidal and toroidal angles, so the toroidal and poloidal half-widths are 60° and 15°, $n_{\rm max}$ is the reference coefficient and it depends on the total particles of the experiment. In this paper, the total amount of Ar is 7×10^{19}, this number is close to the experiment value, and here $n_{\rm max}$ is selected about 2×10^{22}. As shown in Fig. 2, the gas injection port is located at toroidal 0° and poloidal −90° (yellow area in the profile). Figures 2(a)–2(c) show the initial Poincare plots of three cases: case 1, $\Phi_{2/1} = 330°$, $\Phi_{3/1} = 90°$; case 2, only $\Phi_{2/1} = 330°$; and case 3, $\Phi_{2/1} = 330°$, $\Phi_{3/1} = 270°$. Case 2 is regarded as a reference case. The phase of pre-existing island is defined as the toroidal phase of the O-point of the magnetic island relative to the gas injection port when they share the same initial poloidal angle. The O-point phase is determined by finding the minimum value of B_θ. Figure 2(d) shows the temporal evolution of confined REs in the disruption process for the above three cases. The RE suppression can be achieved in case 3. For case 1, a considerable number of REs in the plasma region at the end of TQ duration exists, and the number of left REs is similar to the case of only $\Phi_{2/1} = 330°$.

Detailed calculation results are given to understand the influence of the relative phase of $3/1$ and $2/1$ magnetic islands on the loss of REs. There are four types of cases in all: (i) 12 cases of multiple modes, in which the phase of the pre-existing $3/1$ magnetic island is changeable and the phase of $2/1$ magnetic island is fixed; (ii) 12 cases with only $3/1$ magnetic island whose phase is changeable; (iii) 1 case with only $2/1$ magnetic island whose phase is fixed; (iv) 1 case with no pre-existing island (as a comparison). All of cases are shown in Fig. 3, the calculation results indicate that under the condition of MGI trigger disruption, the relationship of the relative phase between the pre-existing $2/1$ and $3/1$ magnetic islands and the confined remaining REs at the end of the TQ phase is predicted to be approximately sinusoidal theoretically. The red curve is fitted by the first-order Fourier expansion. The final confined ratio of REs in the reference case without pre-existing magnetic island is approximately 0.32. The case of only $2/1$ magnetic island is 0.48, the case of $\Phi_{2/1} = 330°$, $\Phi_{3/1} = 90°$ (case1) is 0.51, and the case of $\Phi_{2/1} = 330°$, $\Phi_{3/1} = 270°$ is only 0.07. Compared with that of only $2/1$ magnetic island, the cases of $2/1$ magnetic island coupled with $3/1$ magnetic island can affect the suppression of REs significantly.

According to the distribution of the magnetic field lines (MFLs) at the initial position of poloidal plane, we have selected MFLs from different radial positions for tracking and given the Poincare evolution of the MFLs at different radial positions to compare easily the evolution of the magnetic topological structure between case 1 and case 3. In this paper, two different normalized radial positions (r/a) are selected, where a is denoted as the minor radius of J-TEXT tokamak. $r/a = 0$ (magnetic axis position) and $r/a = 0.25$ (core position) are present.

The trajectories of MFLs of three typical cases at $r/a = 0$ and $r/a = 0.25$ are given in Figs. 4 and 5, respectively. From the comparison of the MFL trajectory between case 1 and case 3 at the initial TQ time, the point number of MFLs outside LCFS of case 1 is significantly higher than that of case 3 at $r/a = 0$ and $r/a = 0.25$ before 0.6 ms. Therefore, the initial phase between different magnetic islands leads to the evolution of different magnetic topologies during disruption, and the magnetic surface in case 3 ($\Phi_{2/1} = 330°$, $\Phi_{3/1} = 270°$) is more stochastic.

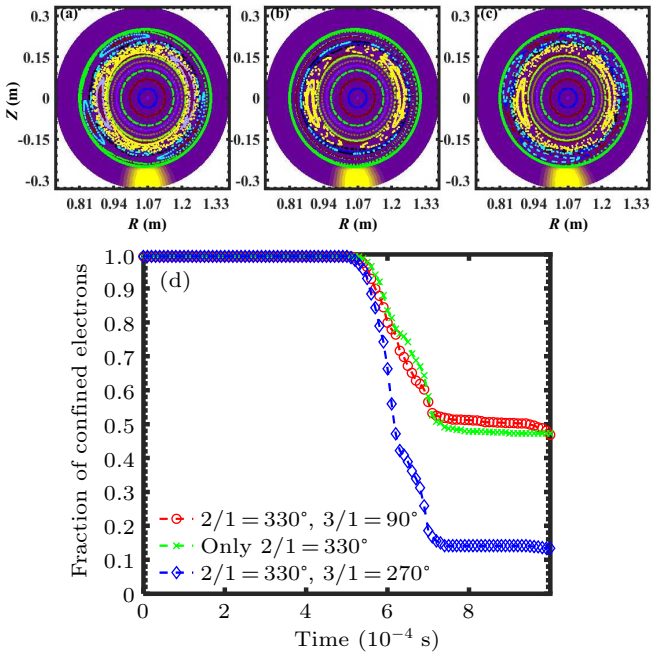


Fig. 2. Poincare plot of magnetic lines corresponding to (a) $\Phi_{2/1} = 330°$, $\Phi_{3/1} = 90°$ case, (b) $\Phi_{2/1} = 330°$ case, (c) $\Phi_{2/1} = 330°$, $\Phi_{3/1} = 270°$ case at the initial time. The yellow magnetic line mainly locates near the $q = 2/1$, and the blue magnetic line mainly locates near the $q = 3/1$, the green circle is the position of LCFS. (d) The fraction of confined REs vs. time (ms).

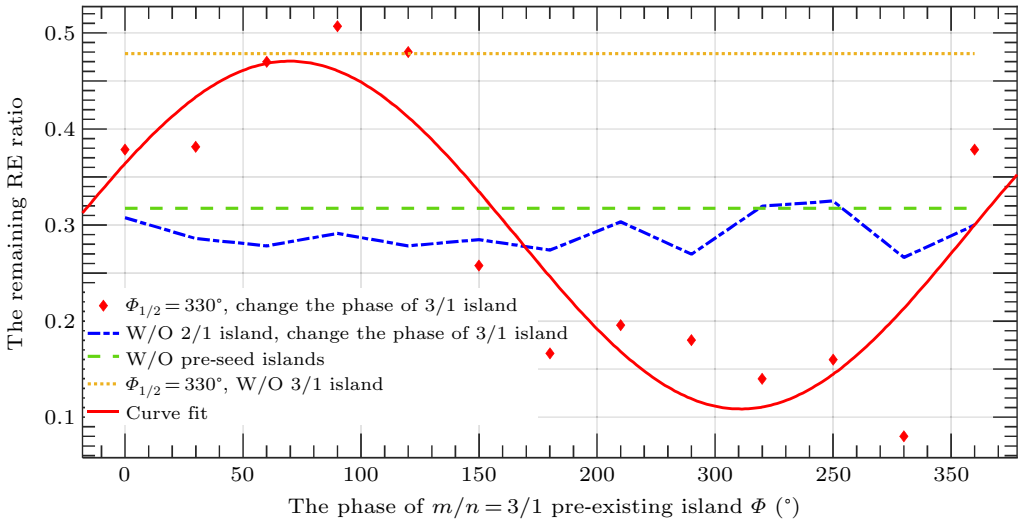


Fig. 3. Dependence of the ratio of remaining REs on the toroidal phase of pre-existing $3/1$ magnetic island with the phase of $2/1$ magnetic island fixed (solid red line). Dependence of the remaining RE ratio on the toroidal phase of only pre-existing $3/1$ magnetic island (blue dash-dot line). The remaining RE ratio of without pre-existing island during the disruption (green dash line). The remaining ratio of RE during the disruption of only $\Phi_{2/1} = 330°$ (yellow dot line).

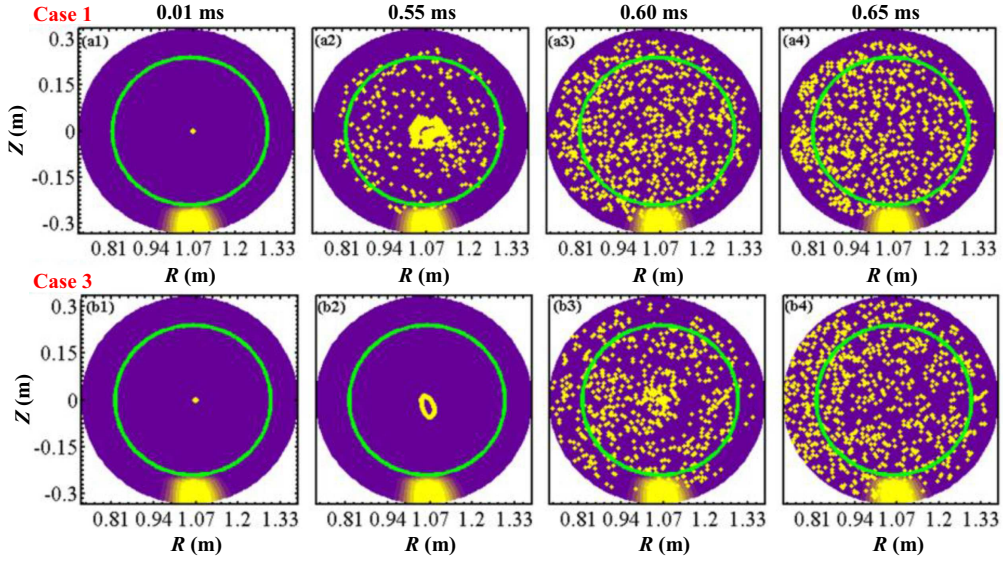


Fig. 4. Poincare plots for MFLs at $r/a = 0$ of case 1 and case 3.

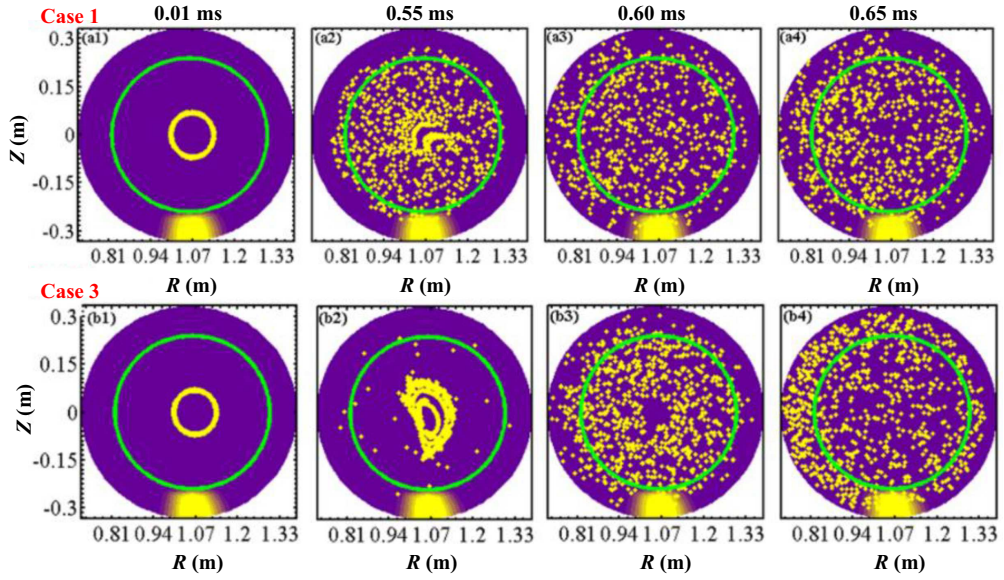


Fig. 5. Poincare plots for MFLs at $r/a = 0.25$ of case 1 and case 3.

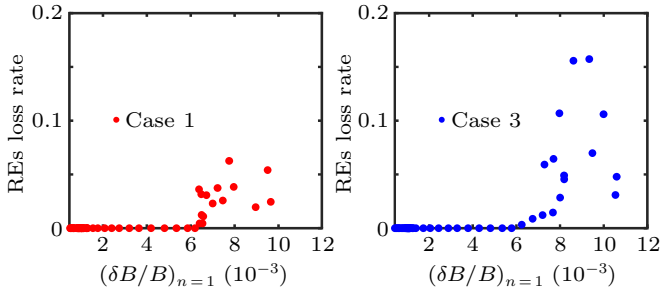


Fig. 6. Relationship between $\delta B/B$ (calculated from the formula $\delta B/B \approx \sqrt{W_{\mathrm{mag},n}/W_{\mathrm{mag},0}}$, it includes all of the magnetic perturbations of plasma) and RE loss rate during 0 ms–0.66 ms for (a) case 1 and (b) case 3.

Theoretical and experimental results indicate that the RE loss has a certain magnetic perturbation threshold. From the data of magnetic perturbation level in simulation, we can get relationship between the RE loss rate and magnetic perturbation level (Fig. 6). Case 1 and case 3 almost have the same magnetic perturbation threshold of RE loss, but the RE loss rate of case 3 is higher than that of case 1 at same value of $\delta B/B$ from the initial moment to the end of TQ. As a result, the number of confined REs in case 1 is still high enough at the end of TQ. The evident difference in the RE loss rate cannot be explained by the value of magnetic perturbation of toroidal modes directly.

3.2. Correlation between the impurity flux to the core region and the RE loss

In this paper, in order to study the penetration process of Ar into the plasma region under the three above cases, the distributions of the quantity of ionized Ar in different radial positions (r/a is the radial normalized radius, where a is denoted as the minor radius of the J-TEXT tokamak) at $t = 0.55$ ms, 0.60 ms, and 0.65 ms are given in Fig. 7. It can be seen from Fig. 7(a) that the Ar in these three cases has transported from the boundary to the core of the plasma and deposited near the $q = 2$ surface at $t = 0.55$ ms. The amount of ionized Ar of case 3 is more than that of case 1 in the position of $q = 2$ surface. After $t = 0.60$ ms, Ar has penetrated into the core region of plasma (inside $r/a = 0.5$) in case 3, while in the others two cases, Ar has not reached the core region. Therefore, through the comparison it can be obtained that the penetration rate of impurity gas in case 3 into the plasma core is faster during TQ of disruption.

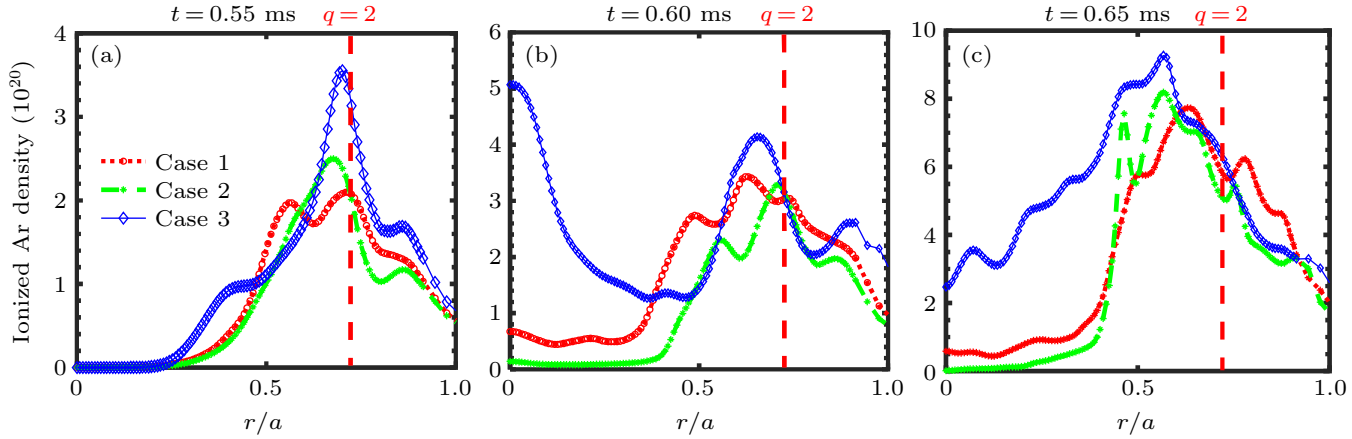


Fig. 7. Radial distribution of total amount of ionized argon at three time points: (a) $t = 0.55$ ms (pre-TQ), (b) $t = 0.60$ ms (TQ), (c) $t = 0.65$ ms (TQ). The red dotted line is case 1, the green dotted line is case 2, and the blue solid line is case 3. The radial position of $q = 2$ surface is about $r/a = 0.72$, which shown by the vertical red line.

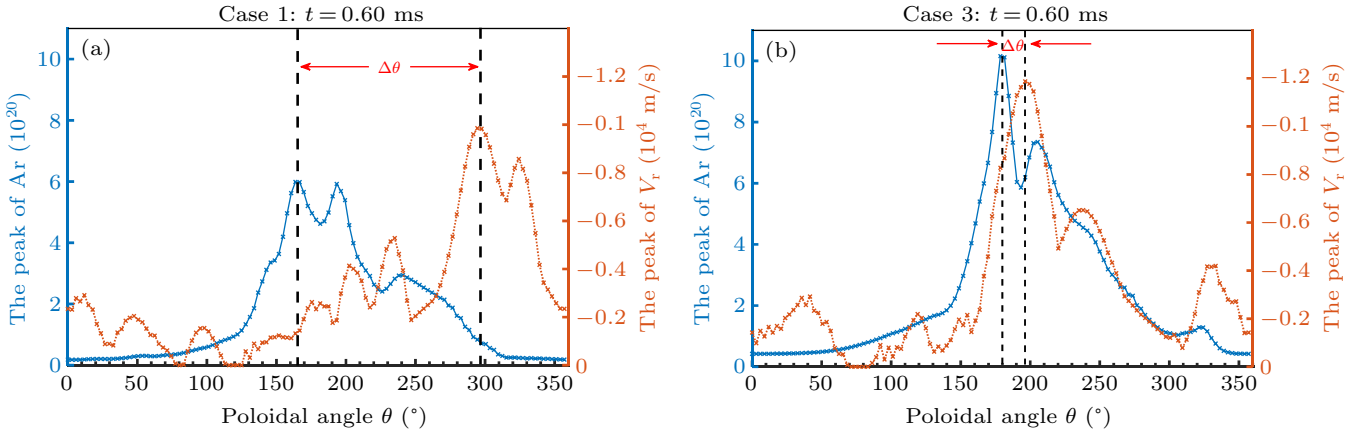


Fig. 8. Distribution of Ar (blue curve) and impurity flow velocity V_r (orange curve) in poloidal angle of (a) case 1 and (b) case 3. $\Delta\theta$ shows the phase difference of poloidal angle between the peak value of ionized Ar and the peak value of V_r.

When the value of the radial impurity flow velocity, denoted by V_r, is negative, the impurity (like Ar) spreads towards the plasma core region. The poloidal distribution of the magnitude of Ar and its flow velocity V_r in case 1 and case 3 at the toroidal position of MGI are shown in Fig. 8. It can be seen that at 0.60 ms, the phase difference of poloidal angle $\Delta\theta$ between the peak value of ionized Ar and the peak value of V_r is smaller in case 3, while the phase difference in case 1 is larger. This phase difference $\Delta\theta$ will affect the radial penetration process of Ar from the boundary to the core and the deposition effect of ionized Ar in the plasma to a great extent. The radial penetration for the Ar is easier with the smaller phase difference.

The pre-seed magnetic islands can destroy the magnetic topology effectively, the penetration of Ar into the core region is affected by the relative phase of $2/1$ magnetic island and $3/1$ magnetic island. The variations of the amount of Ar which has already penetrated into $q = 2$ (q is the safety factor) magnetic surface of case 1 and case 3 are shown in Fig. 9. In the range of 0.6 ms–0.7 ms, the growth rate of Ar impurity which penetrates inside $q = 2$ surface in case 3 is significantly larger than that in case 1. The process of impurity penetration in the core region is beneficial for the enhancement of the magnetic topology stochasticity degree and then for the loss of REs.

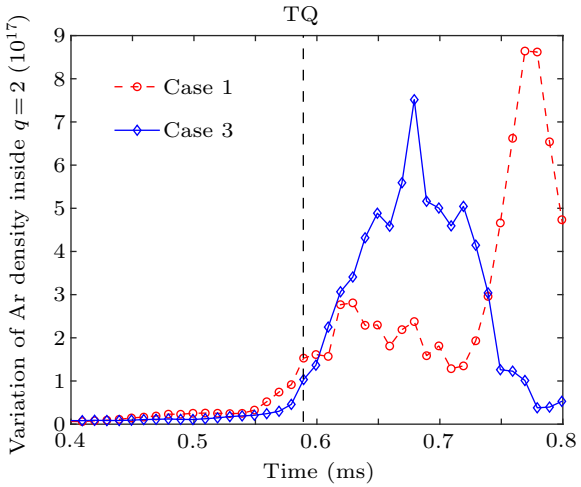


Fig. 9. Temporal evolution of variation of ionized Ar inside $q = 2$.

4. Discussion and conclusion

This paper has predicted the RE suppression through pre-existing magnetic island coupling with the NIMROD code. The experiments of multimode coupling through mixed modes of RMP on suppressing REs have also been carried out on J-TEXT. Preliminary results are obtained, but experimental data are not available. Results indicate that the relative phase difference between $2/1$ and $3/1$ magnetic islands has a remarkable effect on the RE transport during the TQ stage. Under the parameters of the J-TEXT tokamak, the relationship of the relative phase between pre-existing $2/1$ and $3/1$ magnetic islands and the confined remaining REs at the end of the TQ phase is predicted to be approximately sinusoidal theoretically. An optimal phase exists between multimode magnetic islands, which makes the REs almost expelled from the plasma region. This result is from the initial phase between different magnetic islands lead to the evolution of different magnetic topologies during disruption. Although the amplitude differences of magnetic perturbation are limited under different phase conditions, the magnetic surface in case 3 ($\Phi_{2/1} = 330°$, $\Phi_{3/1} = 270°$) is stochastic and conducive to expel REs outside of plasma region.

Case 3 which has the more stochastic magnetic surface to expel REs is related to the impurity transport characteristics under the different phase between the $2/1$ and $3/1$ islands. The results show that when the MGI is used to trigger the disruption under different relative phases of multiple magnetic islands, the penetration process and deposition effect of Ar impurity in the plasma regions are different. And the magnetic perturbation level ($\delta B/B$) depends greatly on the total impurities of the core region, so this finally affects the dynamic transport of REs. The simulation results imply that the impurity is easier to spread into the core region with smaller phase difference of $\Delta\theta$ between the peak value of ionized Ar density and the peak value of V_r. Unlike our previous research work,[33] the impurity transport mechanism here is more likely to come from $\boldsymbol{E} \times \boldsymbol{B}$ perpendicular convection of plasma and leads to the radial flow of impurities. However, to clarify the final transport mechanism, we need to further analyze the generation mechanism of radial flow under the condition of pre-seeded multi-modes, this is our next work.

Acknowledgments

Project supported by the National Natural Science Foundation of China (Grant Nos. 12175078 and 51821005). The authors are very grateful for the assistance of the NIMROD team.

References

[1] Hender T C, Wesley J C, Bialek J, Bondeson A, Boozer A H, Buttery R J, Garofalo A, Goodman T P, Granetz R S and Gribov Y 2007 *Nucl. Fusion* **47** S128
[2] Wesson J A, Gill R D, Hugon M, Schüller F C, Snipes J A, Ward D J, Bartlett D V and Campbell D J 1989 *Nucl. Fusion* **29** 641
[3] Arnoux G, Loarte A and Riccardo V 2009 *Nucl. Fusion* **49** 085038
[4] Lehnen M, Aleynikova K, Aleynikov P B, Campbell D J, Drewelow P, Eidietis N W, Gasparyan Y, Granetz R S, Gribov Y and Hartmann N 2015 *J. Nucl. Mater.* **463** 39
[5] Matthews G F 2016 *Phys. Scripta* **T167** 014070
[6] Riccardo V and JET EFDA contributors 2003 *Plasma Phys. Control. Fusion* **45** A269
[7] Baylor L R, Barbier C C, Carmichael J R, Combs S K, Ericson M N and Bull N D E 2017 *Fusion Sci. Technol.* **68** 211
[8] Rosenbluth M N and Putvinski S V 1997 *Nucl. Fusion* **37** 1355

[9] Taylor P L, Kellman A G, Evans T E, Gray D S, Humphreys D A, Hyatt A W, Jernigan T C and Lee R L 1999 *Phys. Plasmas* **6** 1872

[10] Commaux N, Baylor L R, Jernigan T C, Hollmann E M, Parks P B, Humphreys D A, Wesley J C and Yu J H 2010 *Nucl. Fusion* **50** 112001

[11] Pautasso G, Fuchs C J, Gruber O, Maggi C F, Maraschek M, Pütterich T, Rohde V, Wittmann C, Wolfrum E, Cierpka P and Beck M 2007 *Nucl. Fusion* **47** 023

[12] Commaux N, Shiraki D, Baylor L R, Hollmann E M, Eidietis N W and Lasnier C J 2016 *Nucl. Fusion* **56** 046007

[13] Reux C, Bucalossi J, Saint-Laurent F, Gil C, Moreau P and Maget P 2010 *Nucl. Fusion* **50** 095006

[14] Pautasso G, Mlynek A, Bernert M, Mank K, Herrmann A, Dux R, Müller H W, Scarabosio A and Sertoli M 2015 *Nucl. Fusion* **55** 033015

[15] Bozhenkov S A, Lehnen M, Finken K H, Jakubowski M W, Wolf R C, Jaspers R, Kantor M, Marchuk O V, Uzgel E and Wassenhove G V 2008 *Plasma Phys. Control. Fusion* **50** 105007

[16] Shiraki D, Commaux N, Baylor L R, Eidietis N W, Hollmann E M, Izzo V A, Moyer R A and Paz-Soldan C 2015 *Nucl. Fusion* **55** 073029

[17] Chen Z Y, Huang D W, Luo Y H, Tang Y, Dong Y B, Zeng L, Tong R H, Wang S Y, Wei Y N and Wang X H 2016 *Nucl. Fusion* **56** 112013

[18] Hollmann E M, Baylor L R, Jernigan T C, Hollmann E M, Humphreys D A, Wesley J C and Izzo V A 2010 *Phys. Plasmas* **17** 056117

[19] Tokuda S and Yoshino R 1999 *Nucl. Fusion* **39** 1123

[20] Papp G, Drevlak M, Fülöp T, Helander P and Pokol G I 2011 *Plasma Phys. Control. Fusion* **53** 095004

[21] Commaux N, Baylor L R, Combs S K, Eidietis N W, Evans T E, Foust C R, Hollmann E M, Humphreys D A and Izzo V A 2011 *Nucl. Fusion* **51** 103001

[22] Lehnen M, Bozhenkov S A, Abdullaev S S, TEXTOR Team and Jakubowski M W 2008 *Phys. Rev. Lett.* **100** 255003

[23] Yoshino R and Tokuda S 2000 *Nucl. Fusion* **40** 1293

[24] Gobbin M, Li L, Liu Y Q, Marrelli L, Nocente M, Papp G, Pautasso G, Piovesan P, Valisa M and Carnevale D 2018 *Plasma Phys. Control. Fusion* **60** 014036

[25] Chen Z Y, Huang D W, Izzo V A, Tong R H, Jiang Z H, Hu Q M, Wei Y N, Yan W, Rao B and Wang S Y 2016 *Nucl. Fusion* **56** 074001

[26] Lin Z F, Chen Z Y, Huang D W, Huang J, Tong R H, Wei Y N, Yan W, Li D, Hu Q M and Huang Y 2019 *Plasma Phys. Control. Fusion* **61** 024005

[27] Lin Z F and Chen Z Y 2019 *Annual Report IFPP*

[28] Jiang Z H, Huang J, Tong R H, Yang T T, Lin Z F, Izzo V, Li C H and Liang Y F 2019 *Phys. Plasmas* **26** 062508

[29] Sovinec C R, Schnack D D, Pankin A Y, Brennan D P, Tian H, Barnes D C, Kruger S E, Held E D, Kim C C, Li X S, Kaushik D K, Jardin S C and the NIMROD Team 2005 *J. Phys.* **16** 25

[30] Izzo V A, Whyte D G, Granetz R S, Parks P B, Hollmann E M, Lao L L and Wesley J C 2008 *Phys. Plasmas* **15** 056109

[31] Izzo V A, Hollmann E M, James A N, Yu J H, Humphreys D A, Lao L L and Parks P B 2011 *Nucl. Fusion* **51** 063032

[32] Izzo V A and Parks P B 2017 *Phys. Plasmas* **24** 056102

[33] Jiang Z H, Yang T T, Yuan J J, Li C H, Ye X, Huang J, Liang Y and Izzo V A 2020 *Nucl. Fusion* **60** 066004